Focused Tomography: Reducing CT Radiation Exposure for Region of Interest Viewing

Timothy E. Olson and Stephanie M. Leon

***Abstract*— Physicians ordering CT scans are often interested only in an anatomical region of interest (ROI), such as the spine or hip. Even if the reconstructed field of view is reduced to the ROI, traditional reconstruction algorithms require equal radiation exposure throughout the axial of the body to produce an accurate reconstruction, resulting in the irradiation of organs and tissues that are not of clinical interest. This work presents Focused Tomography, a modified filtered back-projection (FBP) algorithm that permits accurate reconstruction of a limited FOV with a 90% or greater reduction of radiation exposure outside the clinical ROI. This improvement is possible because only the low-frequency components of the off-ROI data are required for accurate reconstruction, and these are largely unaffected by noise. The algorithm was tested using CT images of a cadaver acquired with radiation doses of 17 mGy within the ROI and 1.7 mGy outside of the ROI. ROIs using the new algorithm were compared to the original 17 mGy image, with near-perfect preservation of spatial resolution and Hounsfield units. Trials with additional simulated noise suggest that even lower off-ROI doses would suffice. Current CT machines do not have a mechanism to reduce the radiation delivered to areas outside of an ROI; however, with this development of the mathematical basis for focused reconstruction, the engineering of a movable, semi-radiolucent collimator would permit clinical implementation.**

***Index Terms*— Computed tomography, reconstruction algorithm, radiation dose**

T.E. Olson is with the Department of Mathematics, University of Florida, Gainesville, FL 32610 USA (e-mail: olsontch@ufl.edu).

S.M. Leon is with the Department of Radiology, University of Florida, Gainesville, FL 32610 USA (e-mail: leons@radiology.ufl.edu).

This work has been patented by The University of Florida: Timothy Edward Olson and Stephanie Marie Leon, Focused Tomography (U.S. Patent Application No. 16/986,014 filed August 5, 2020). U.S. Patent and Trademark Office.

I. Introduction

COMPUTERIZED Tomography (CT) has become a standard diagnostic tool in modern medicine. In the last 30 years, however, CT use has become so prevalent that the cumulative radiation dosage which patients are exposed to during their lifetime has increased dramatically [1], leading to much speculation about the potential population-level effects of increasing radiation exposure.

Oftentimes the clinical focus of a CT scan is a limited Region of Interest (ROI) which has been identified through clinical means or previous imaging; for some study types, such as spinal imaging, the reconstructed image is restricted to this limited field of view (FOV). However, current CT technology is unable to restrict the *radiation exposure* to an ROI, and all tissues within the axial plane are exposed, even if they are not of clinical interest. This limitation is due primarily to the reconstruction algorithms used, which require information about all attenuating objects within each projection to produce accurate reconstructions. Thus, data from the entire axial slice must be collected, even if it will not be displayed in the final image. Although the technology to limit radiation exposure outside of the clinical ROI could certainly be developed, there is little incentive to do so unless reconstruction algorithms can cope with the loss of data.

This work presents a modified filtered back-projection (FBP) algorithm that permits accurate reconstruction of a limited FOV with substantial reduction of radiation exposure outside the clinical ROI. Because modern iterative reconstruction algorithms generally start from an initial "guess" generated by FBP, this novel algorithm would also be beneficial for most implementations of iterative reconstruction.

Historical Background

Local tomography, the ancestor of the algorithm presented here, was first investigated in the early 1990's. However, these early investigations preserved the edges but not the pixel values of the image, instead returning a transformed image [2]. Because the pixel values in CT are "Hounsfield units" (HU) that have a physical meaning related to the attenuation properties of the tissues, preservation of these values is important. HU measurements are used by radiologists to characterize tissues, and are also important for specialized applications including material identification in dual-energy CT and attenuation correction in hybrid imaging, among other applications.

Subsequent improvements to localized tomography were able to preserve the original pixel values [3-4]. This is possible when one realizes that the low-frequency components of the image are the only components which need non-local x-rays (i.e., those that do not intersect the ROI) for their estimation. The high-frequency components can be measured with the local line integral measurements which pass through the ROI (Fig. 1). Thus, one does not need to send radiation on paths which do not intersect the ROI to find the high-frequency components of the image.

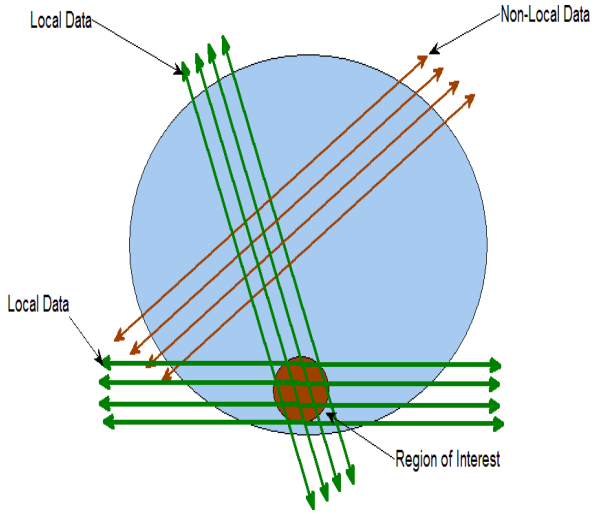

Fig. 1. Stylized illustration of a typical scenario for localized tomography. The Region of Interest (ROI) is shown as a brown circle within the larger blue circle that represents entire CT slice. Green arrows represent "local" x-ray paths which pass through the ROI. Red arrows represent "non-local" x-ray paths which do not pass through the ROI.

In order to provide a complete and accurate reconstruction of the ROI, two methods were presented which, featured a) Regular sampling of local x-rays through the ROI, in order to reconstruct the high-frequency components of the image, and b) Sparse sampling of non-local x-rays, allowing for the recovery of low frequency components of the image. The combination of these methods resulted in an accurate reconstruction of the ROI, with the potential for greatly reduced radiation dosages [3], [4].

Many other methods have been presented since these initial works [6-10]. These methods work very well but only allow binary sampling, i.e., either an x-ray is measured along a line integral or it is not. Unfortunately, this idea of "skipping" line integrals has no technological parallel that would permit a practical reduction in radiation dose, as x-ray tubes do not produce radiation in such a manner. Thus, an algorithm must be designed that has a practical corollary that can be applied to physical CT systems.

This work proposes a third method, which allows variable sampling of the x-rays to permit a dramatically reduced radiation flux through the portions of the body outside of the ROI. The lower doses applied outside of the ROI will be sufficient because they will only be utilized to determine the low-frequency components of the image. Thus, the lower signal- t o- noise ratio (SNR) measurements can be averaged, producing adequate SNR measurements for these low-frequency components. On the other hand, the tissues within the ROI will be exposed to the usual radiation dose typical of standard clinical imaging, allowing the detailed, high-frequency components of the image to retain standard SNR measurements.

Theoretical Background

CT data is generally collected in a helical fan-beam geometry; however, for the discussion of the reconstruction process, we will assume that this data has been reformatted into a parallel beam data set. Thus we assume that the data can be viewed as a function of two variables, angle θ and distance r from the origin, or that the data P_f from each projection has the form

$$P_f(r,\vec{\theta}) = \int f\left(r\vec{\theta} + t\vec{\theta}^{\perp}\right)dt, \qquad (1)$$

where t is an arbitrary variable chosen for the purposes of integration (Fig. 2).

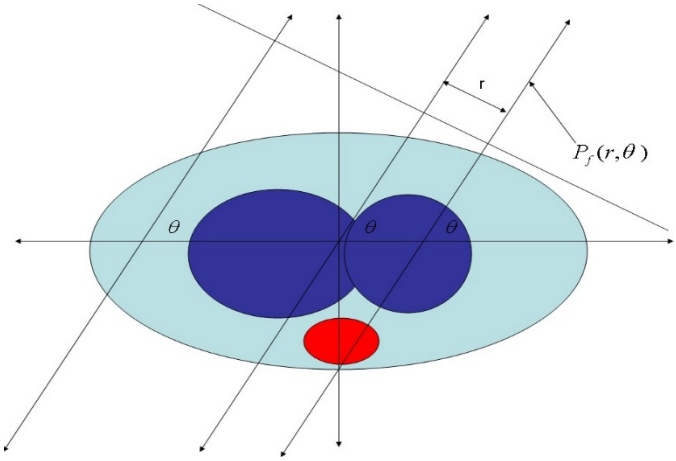

Fig. 2. Illustration of the projection angles, coordinates, and vectors referred to in (1).

The natural coordinates for tomography are $x = r\vec{\theta} + t\vec{\theta}^{\perp}$. Moreover $\vec{x}\cdot\vec{\theta}^{\perp} = r$. We want to see what the Fourier coefficients propagating at a fixed direction θ have in common with the projections, so we consider

$$\hat{f}\left(s\vec{\theta}\right) = \frac{1}{2\pi}\int P_f(r,\vec{\theta})e^{irs}dr, \qquad (2)$$

where s is radial polar component of the polar representation of the Fourier transform.

Thus, a central slice of the two-dimensional Fourier transform of $f(x,y)$, i.e. $\hat{f}\left(s\vec{\theta}\right)$, can be obtained from the one -dimensional projections of the function, or $P_f(r,\vec{\theta})$. This is the Radon Transform, which can be written:

$$\mathcal{F}_1\left(P_f(r,\vec{\theta})\right) = \frac{1}{2\pi}\hat{f}\left(s\vec{\theta}\right). \qquad (3)$$

From (3), we can derive the formula for filtered back-projection (4), which uses $|w(s)|$ as a frequency cut-off window.

$$f(\vec{x}) \approx \frac{1}{2\pi}\int_0^{\pi}\int_{-\infty}^{\infty}\hat{f}(s\vec{\theta})\,|s|\,w(s)e^{irs}dsd\theta$$
$$= \int_0^{\pi}\left(P_f(r,\vec{\theta}) * \mathcal{F}^{-1}(|s|\,w(s))\right)(\vec{x}\cdot\vec{\theta})d\theta \quad (4)$$

By choosing $w(s)$ appropriately we can make the approximation above arbitrarily small. If we denote $\mathcal{F}^{-1}(|s|\,w(s)) = k(r)$ then, by the convolution theorem, we have:

$$f(\vec{x}) \approx \int_0^{\pi}\left(P_f(r,\vec{\theta}) * k(r)\right)(\vec{x}\cdot\vec{\theta})d\theta\,. \quad (5)$$

One problem with (5) is that the kernel $k(r)$ is very broad as a function of r, due to the jump discontinuity of the derivative of the function $|s|$ at the origin. As a result, radiation measurements would be required far from the ROI.

This problem can be solved by separating the discontinuity at the origin of $|s|$ into separate portions: $|s|w_2(s)$ at the origin, and $|s|(1-w_2(s))$ away from the origin. The corresponding inverse Fourier transforms will involve two terms: a low-frequency kernel $k_l(r)$, which is the inverse Fourier transform of $|s|w_2(s)$, and a high-frequency kernel $k_h(r)$, which is the inverse Fourier transform of $|s|(1-w_2(s))$. Thus, $k(r) = k_l(r) + k_h(r)$, and (5) can be re-written:

$$f(\vec{x}) = \int_0^{\pi}\left(P_f(r,\vec{\theta}) * k_l(r)\right)(\vec{x}\cdot\vec{\theta})d\theta\; +$$
$$\int_0^{\pi}\left(P_f(r,\vec{\theta}) * k_h(r)\right)(\vec{x}\cdot\vec{\theta})d\theta\,, \quad \text{or}$$
$$f(\vec{x}) = f_l(\vec{x}) + f_h(\vec{x}). \quad (6)$$

The kernels are illustrated in Fig. 3. The energy of $k_h(r)$ is contained within the interior 9 pixels of the current 512-pixel digitization to an accuracy of 1/10000. The energy concentration of $k_l(r)$, similarly measured, takes 175 terms. Thus, the low-frequency terms require a great deal of non-local information, and the high-frequency terms can be measured locally.

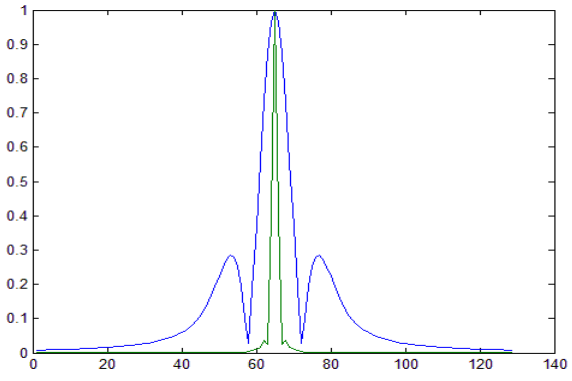

Fig. 3. The kernel decompositions $k_l(r)$ and $k_h(r)$ are shown in blue and green, respectively.

Initially there seems to be no advantage to decomposing $k(r)$ into two kernels from a radiation reduction standpoint, since the low-frequency kernel still requires gathering large quantities of data from outside the ROI. To understand the benefit, consider the structure theorem for the projections or Radon transform, which states that:

$$P_f(r,\vec{\theta}) = (1-r^2)^{-1/2}\sum_{l=0}^{\infty}T_l(r)h_l(\theta), \quad (7)$$

where $T_l(r)$ are the Chebyshev polynomials. Taking the Fourier transform of this yields:

$$\hat{f}(s\vec{\theta}) = P_f(\theta,s) = \left(\frac{\pi}{2}\right)^{-1/2}\sum_{l=0}^{\infty}i^{-1}J_l(s)h_l(\theta)$$
$$= \left(\frac{\pi}{2}\right)^{-1/2}\sum_{l=0}^{N-1}i^{-1}J_l(s)h_l(\theta) +$$
$$\left(\frac{\pi}{2}\right)^{-1/2}\sum_{l=N}^{\infty}i^{-1}J_l(s)h_l(\theta)$$
$$= \hat{f}_l(s,\theta) + \hat{f}_h(s,\theta), \quad (8)$$

where $J_l(s)$ are the Bessel functions, and $h_l(\theta)$ is a trigonometric polynomial of order l.

The key to understanding (8) is that the low-frequency terms in s, which are the Bessel functions, are only multiplied in frequency by the low-order terms $h_l(\theta)$. Thus, we do not have to measure the low-frequency terms for many angles θ in order to accurately determine the complete low-frequency components of the image.

The approach of Localized Tomography espoused in [3], [4] suggested sampling the sinogram outside the ROI at a limited number of angles, while sampling the ROI at all angles. Essentially, the method would require a narrow, linear x-ray beam similar to those found in the earliest CT machines of the 1970's, which could be sampled or not as needed. However, this approach cannot be implemented on modern CT machines. Firstly, the sampling theory is based on an axial parallel-beam geometry which does not exist; modern scanners use fan beams or cone beams, most often with helical scanning. Secondly, the x-ray tube cannot shut off or modulate individual "rays" of the beam to permit full sampling of the ROI with a reduced number of angles sampled outside the ROI. Thus, refinements to the technique are required to make the approach feasible.

Proposed Refinements to the Theory

Rather than utilizing a standard x-ray flux at a limited number of angles for off-ROI imaging, an alternative would be to sample all angles with a lower flux. We call this approach "Focused Tomography" to differentiate it from the earlier attempts at localized tomography. This scenario would likewise save dose, but in contrast to earlier proposals, could be implemented on physical systems with arbitrary geometries. Movable attenuating filters, described in more detail in the Discussion, could be used to accomplish this off-ROI dose reduction while permitting the full dose to be used within the ROI.

To illustrate this approach mathematically, we will assume for now that the ROI is circular with radius r_1, and for simplicity that the x-ray tube is centered on the center of the circle when $\theta = 0$. There is a distance d from the isocenter of the scanner to the center of the ROI. As the x-ray tube moves with θ, the center of the circle will then be a distance $d(\theta) = d\sin\theta$ off of the center of the gantry. Thus we want to gather a full data set of the x-rays which pass through the ROI, which represent our first data set:

$$P_f^h(\theta,r) = P_f(\theta,r) \tag{9}$$

where $0 \le \theta \le \pi$ and $r \in [d\sin\theta - r_1, d\sin\theta + r_1\,]$. This data set is gathered with full radiation dose, and thus will have a respectively high SNR. The notation $P_f^h(\theta,r)$ recognizes that this data will be used to reconstruct the high frequency details of the image.

A second data set is then gathered from all of the lines or projections which did not intersect the region of interest. This is our low frequency data set:

$$P_f^l(\theta,r) = P_f(\theta,r) \tag{10}$$

where $0 \le \theta \le \pi$ and $r \notin [d\sin\theta - r_1, d\sin\theta + r_1\,]$. This data set is gathered with minimal radiation, and will have very low SNR. This data will only be needed to reconstruct the low frequency portion of the image, however, and will not affect the final image in the ROI, however.

We now simply combine the data sets to get our approximate, noisy sinogram or Radon transform:

$$P_f(\theta,r) = P_f^h(\theta,r) + P_f^l(\theta,r), \tag{11}$$

noting that we have sampled all of the Radon transform, some of it at high SNR and some at low SNR. Referring to (6), we see that our final reconstruction will be:

$$\begin{aligned} f(\vec{x}) = \int_0^\pi \Big(P_f^h(r,\theta) * k_h(r) + \\ P_f^l(r,\theta) * k_h(r)\Big)\big(\vec{x}\cdot\vec{\theta}\big)d\theta \; + \\ \int_0^\pi \Big(P_f^h(r,\theta) * k_l(r) + \\ P_f^l(r,\theta) * k_l(r)\Big)\big(\vec{x}\cdot\vec{\theta}\big)d\theta \; . \end{aligned} \tag{12}$$

Let us analyze each term separately. The first term, $P_f^h(r,\theta) * k_h(r)$, will yield most of our high resolution image, and is highly sampled through the ROI. This is the foundation of our reconstruction. The second term, $P_f^l(r,\theta) * k_h(r)$, will be essentially zero, since it is the convolution of high frequency data with a low frequency kernel. The third term, $P_f^h(r,\theta) * k_l(r)$, is essentially zero for the same reason: it is the convolution of low frequency data and a high frequency kernel. The last term, $P_f^l(r,\theta) * k_l(r)$, is the low frequency term which is essential. At first one might think that this would end our ability to accomplish the task of lowering the radiation levels, since these low frequency terms are global and cannot be measured locally. We must remember the structure of the Radon transform to minimize this non-local information.

We have a high-SNR estimate for the high-frequency components inside the ROI. The low-frequency component can be accomplished with the low SNR estimates: recall from (8) that the low-frequency components are only affected by low-frequency sines and cosines with respect to θ, and that

$$\hat{f}_l(s,\theta) = \sum_{l=N}^{\infty} i^{-1} J_l(s) h_l(\theta), \tag{13}$$

with N being very small. Restating this, if you look at the Fourier transform from a polar viewpoint, the small circular components are controlled by very low-order sines and cosines. Therefore, we are estimating very few parameters in the low frequency component. We have a great number of data samples, so the law of large numbers will yield a very solid estimate for the low-frequency component. The purpose of this study is to show that we can accomplish this even if we are gathering this data at very low SNR levels, i.e. with very little radiation.

II. Methods

Initial proof-of-concept trials were performed in Matlab using a simple mathematical phantom (Fig. 4). Projection images of this phantom were created using the "radon" command and subsequently reconstructed using FBP. Fig. 4A displays a reconstructed image with added Poisson noise, with Figs. 4B and 4C demonstrating magnified views of central and inferior sections of 4A, respectively. These can be compared with Figs. 4D and 4E, which show the same regions reconstructed with the proposed method of Focused Tomography with a simulated radiation reduction of approximately 92%. Fig. 4F demonstrates a reconstruction from totally local data, i.e., ignoring the Focused Tomography methodology.

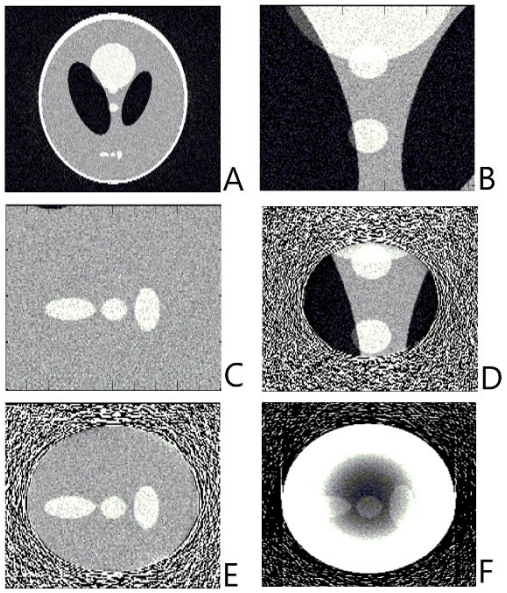

Fig. 4. Results from the mathematical phantom uses in initial trials, showing A) a reconstruction of the entire phantom, B) magnified view of the central section of the phantom image, C) magnified view of the inferior section of the phantom image, D) central portion of the phantom reconstructed with a simulated 92% radiation reduction, E) inferior portion of the phantom reconstructed with a simulated 92% radiation reduction, and F) an attempt at reconstruction using only local data.

Based on the success of these initial attempts, we obtained Institutional Review Board approval to acquire data by imaging human cadavers at different radiation dose levels: a volumetric CTDI ($CTDI_{vol}$) of approximately 1.7 milligray (mGy) and 17 mGy, as calculated by the CT scanner . These will be referred to as the low dose and high dose, respectively. These dose levels were selected because 17 mGy is typical of a clinical CT scan of the torso, and we anticipated that a 10-to-1 ROI/non-ROI dose ratio would perform well with the focused tomography method and represent a sizeable radiation dose reduction.

A Canon Aquilion ONE CT scanner was used to acquire the

images. The different dose levels were obtained by adjusting the mA modulation settings on the scanner, and all other scan techniques were the same as those used in the clinical protocol selected: 120 kV, helical acquisition with pitch of 0.813, 40 mm collimation width, 1-mm slice thickness, and iterative reconstruction with a "body" kernel (FC18).

Because it was not possible to obtain raw projection images from the CT scanner, the reconstructed images were loaded into Matlab and sampled with the "radon" function using 1000 projection angles, The oversampling of angles reduced any numerical errors and is after the fact and numerical in nature.. The data were then re-reconstructed using the Focused Tomography methodology. While the use of processed data is not ideal due to the unavoidable contribution of the original reconstruction algorithm and image processing kernel to the data, this approach still permits the methodology to be tested in a reasonable way to demonstrate proof-of-concept using clinical images.

For this work, we combined images to use high dose for the local (on-ROI) data and the low dose for the non-local, off-ROI data. Production of the composite image is a straightforward substitution of the pixel values from the high-dose data set that correspond to the location of the intended ROI into the low-dose data set; because the pixel values in CT images are already normalized as a function of their attenuation properties rather than their total signal levels, additional normalization between the two data sets was not necessary.

Reductions of the off-ROI dose below one-tenth of the ROI dose might be possible, but the CT scanner we used did not permit further dose reduction below 1.7 mGy. The main effect of lowering the dose in CT is to increase the image noise; thus, we simulated lower doses by simply adding Gaussian noise to the manufactured projections for the off-ROI data. While this is not ideal, the process showed the robustness of the algorithm without being able to obtain original projection data, prior to the logarithmic conversion and original reconstructions by the manufacturer.

Due to the sharp transition in noise levels between the two regions of the image, we also investigated whether it was necessary to include a transition region to avoid artifacts. Thus, we specified two different modes for our images: the first denoted as Focused Tomography 1 (FCT1), which used the lower dosage measurement outside the ROI and the higher dosage measurements inside the ROI, with no transition region between them; and the second denoted as Focused Tomography 2 (FCT2), which used a raised cosine transition window between the lower dosage and the higher dosage measurements.

To ensure that FCT does not create small image differences that are not easily apparent, a difference image was also created in which the data within the ROI of the FCT image was subtracted from the data in the same area of the original image. The difference between the pixel values within the ROI was also calculated as the mean square error (MSE).

III. Results

Fig. 5 demonstrates an ROI positioned on the thoracic spine, at the level of the heart. The original reconstruction

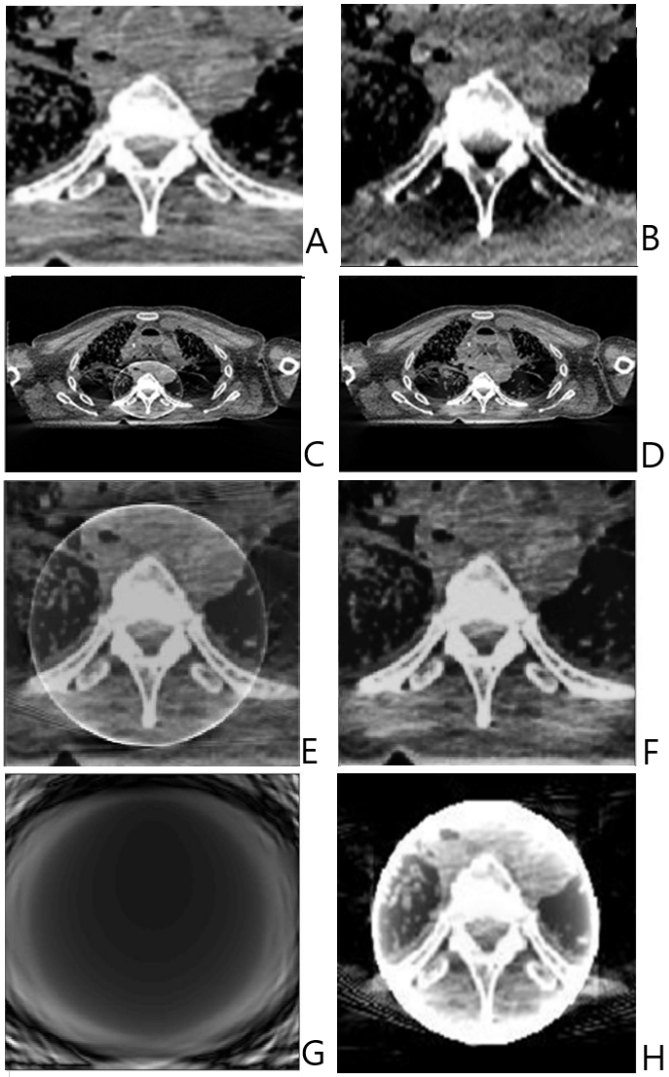

Fig. 5. Results from use of the FCT method to produce an ROI over the thoracic spine, showing A) a magnified view of the original CT scan using 17 mGy, B) a magnified view of the original CT scan using 1.7 mGy, C) the complete reconstruction using FCT1, D) the complete reconstruction using FCT2, E) a magnified view of the ROI using FCT1, and F) a magnified view of the ROI using FCT2, G) the difference image between the original high-dose and FCT reconstructions of the ROI, and H) a reconstruction of an ROI using only local data, for comparison purposes. Notice that A and F are essentially identical in the interior.

with 17 mGy (Fig. 5A) shows typical levels of clinical image quality. The reconstruction with only 1.7 mGy (Fig. 5B) shows a significant loss of detail, increased noise, and shadowing around the spinous process resulting from beam hardening artifact. Figures 5C-F combine these images to demonstrate the FCT methodology on a composite image with high dose in the ROI and low dose outside the ROI. The detail within the ROI is preserved with both the FCT1 and FCT2 methods, although Gibb's ringing is noted around the borders of the ROI using the CT1 method. Inclusion of the transition window with FCT2 removes the appearance of ringing. The difference image between the original high-dose reconstruction and the FCT1 reconstruction shows obvious noise-related differences outside the ROI, but there is no

perceptible difference within the ROI (Fig. 5G). The MSE of this reconstruction was only 0.0041, which is negligible considering that the standard deviation of the pixel values can often exceed 10-20 HU in a uniform background. Fig. 5H shows what the ROI would look like if calculated from local data only, i.e., by neglecting the off-ROI data completely. The severe artifacts apparent in this image would make it unsuitable for clinical use.

The 10-to-1 ROI/non-ROI dose ratio performs well, and it is likely that the algorithm would perform as well at even lower off-ROI doses. Although it was not possible to acquire a CT image with a lower dose than 1.7 mGy, the artificial addition of Poisson noise simulated the effect of using a lower dose outside of the ROI. Both the FCT1 and FCT2 algorithms were tested; Fig. 6 shows the results using FCT1. Even with the addition of so much noise that only the vague outlines of the anatomy are visible through the noise in the off-ROI areas, the image quality within the ROI remains as high as it was in the original image. The MSE was again very low, at 0.00024.

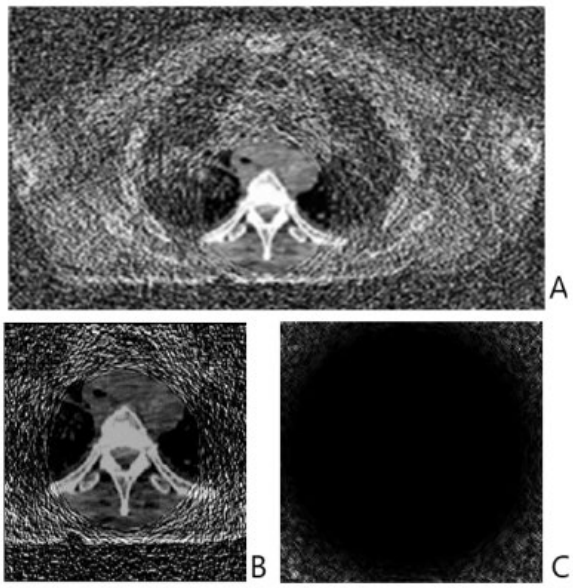

Fig. 6. Results from use of the FCT method with added off-ROI noise, showing A) the complete reconstruction using FCT1, B) a magnified view of the ROI, and C) the difference image between the original high-dose and FCT reconstructions of the ROI

The ROI over the spine shown in Figs. 5-6 is near the isocenter of the CT scanner gantry, but it is not necessary to restrict the method to centrally-placed ROIs. Fig. 7 shows the FCT2 method applied to a CT image of a hip with added noise, demonstrating that the ROI can be placed anywhere within the reconstructed field-of view, even in the high-noise condition.

IV. Discussion

The Focused Tomography method clearly provides a solution to allow reconstruction of an ROI within a CT image with limited data from the regions outside the ROI. All that is needed for accurate reconstruction is the low-frequency information from outside of the ROI, which can be obtained even when there are very high levels of noise. We believe that this success is due to the low-frequency coefficients being nearly invariant on standard human scans. This modification to existing reconstruction algorithms would allow sizeable dose reduction for regions outside the ROI: the data shown using the CT images acquired at 17 mGy and 1.7 mGy

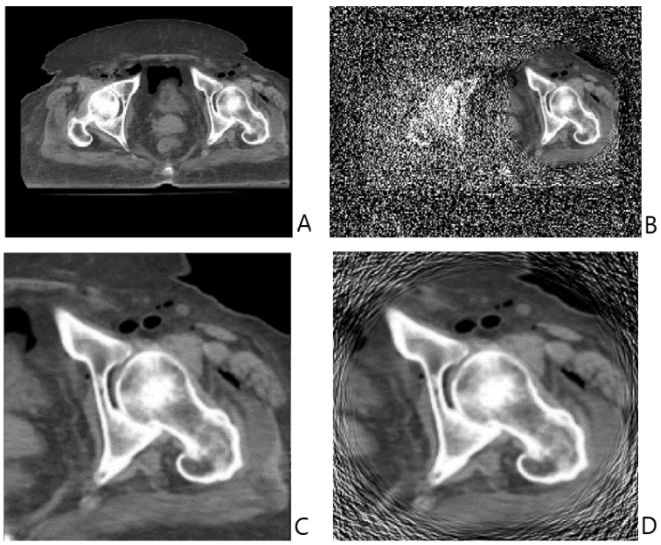

Fig. 7. Results from use of the FCT method for an ROI over the hip, showing A) the original reconstruction, B) the complete reconstruction using FCT2 with added off-ROI noise, C) a magnified view of the hip on the original image, and D) the magnified view of the ROI from B.

demonstrate that a reduction in absorbed dose of ~90% to the off-ROI tissues is certainly possible, and the trials with simulated noise suggest that even lower doses would likely suffice.

The potential to reduce off-ROI dose is of particular interest because reduced field-of-view imaging often includes as "collateral damage" some of the most radiosensitive organs and tissues in the body. For example, spine imaging is one of the most common exams to employ a reduced field of view, but the spine is surrounded by radiosensitive organs including the lungs, stomach, liver, and breast in the thoracic region; and the colon, bladder and reproductive organs in the lumbar regions [6]. Sensitive red bone marrow is also exposed in all areas of spine imaging, e.g. in the shoulders, ribs, sternum, and pelvis. Reduced-radiation imaging of off-ROI regions would likely lower the effective dose the patient receives (and hence, the risk of stochastic effects such as cancer) by an even greater degree than it lowers the absorbed dose. When patients are exposed to multiple CT scans using ROI imaging, as if often the case when evaluating ongoing injuries, treatment options, and outcomes, the benefit multiplies.

Current CT machines do not have a mechanism to reduce the radiation delivered to areas outside of an ROI. However, now that the mathematical basis for reconstruction is understood, the engineering of a movable, semi-radiolucent collimator would permit implementation (Fig. 8). The anatomy to be included within the ROI would be determined by the CT technologist from the anteroposterior and lateral

topograms, which are already acquired as the first step in routine CT scanning. The opening in the collimators would be adjustable from fully open, for traditional unfocused exams, to fully closed, with the position of the opening adjustable laterally. The key is that the collimator is of an appropriately strong material with atomic number and density high enough to block 90-95% of the radiation exiting the bowtie filter through the non-ROI region; the detailed specifications would depend on the beam quality of the most-commonly used x- ray tube potential, but 3-4 mm of tungsten would be a reasonable proposal. This collimator would adjust position to center on the main ROI via continuous motion throughout each rotation of the x-ray tube, allowing full dosage radiation to be gathered from the ROI while shielding the areas outside of the ROI. Implementation of this device will require collaboration with a CT manufacturer.

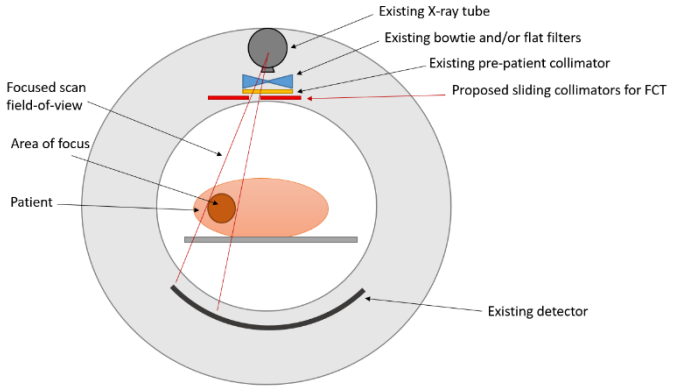

Fig. 8. Drawing of the side view of a CT machine with the gantry cover removed. The proposed movable, semi-radiolucent collimators that would make FCT possible are shown below the bowtie filter and pre-patient collimator.

V. Conclusion

The focused tomography algorithm makes CT imaging of an ROI possible using radiation doses reduced by 90% or more in the off-ROI region. Image quality and Hounsfield unit accuracy within the ROI is essentially unchanged, and the ROI can be located anywhere within the scan field-of-view. This improvement is possible because only the low-frequency components of the off-ROI data are required for accurate reconstruction, and these are largely unaffected by noise. Unlike previous approaches, the FCT algorithm can be implemented on physical systems with arbitrary geometries. With manufacturer support, implementation of FCT on a clinical system could be accomplished by the addition of semi-radiolucent collimators.

References

[1] *NIH Announcement, "Decreasing Patient Radiation Dose from CT Imaging: Achieving Sub-mSv Studies* (U01)".

[2] A. Faridani, E.L. Ritman, K.T. Smith, "*Local Tomography", Vol. 52, # 2, pp. 454-489, SIAM J. Applied Math,* April, 1992.

[3] T. Olson and J. DeStefano, "Wavelet localization of the Radon transform," *IEEE Transactions on Signal Processing, vol. 42, no. 8, pp. 2055-2067,* Aug. 1994, doi: 10.1109/78.301841.

[4] T. Olson, "Optimal Time-Frequency Projections for Localized Tomography", *Annals of Biomedical Engineering*, Vol. 23,622–636 (1995). https://doi.org/10.1007/BF02584461.

[5] D.M. Healy Jr., T. Olson, J.B. Weaver: "*Reduced Motion Artifacts in Medical Imaging by Adaptive Spatio-Temporal Reconstruction*," Numerical Algorithms 9:55-84 (1995).

[6] *The 2007 Recommendations of the International Commission on Radiological Protection*, ICRP Pub lication 103, Annals of ICRP 37 (2-4).

[7] Walnut D. "Applications of Gabor and wavelet expansions to the Radon transform", *Probabilistic and Stochastic Methods in Analysis*, with Applications, edited by J. S. Bymes.Norwell, MA: Kluwer, 1992, pp. 187-205.

[8] Berenstein, C., and D. Walnut. "Local inversion of the Radon transform in even dimensions using wavelets." *Proceedings of the Conference: 75 Years of the Radon Transform*, Vienna, Austria, 1992. Intemational Press, 1994, pp. 38-58.

[9] M. Bhatia, W. C. Karl and A. S. Willsky, "A wavelet-based method for multiscale tomographic reconstruction," in *IEEE Transactions on Medical Imaging, vol. 15, no. 1, pp. 92-101, Feb. 1996*, doi: 10.1109/42.481444.

[10] Tai-Chiu Hsung and D. P. K. Lun, "New sampling scheme for region-of-interest tomography," in *IEEE Transactions on Signal Processing, vol. 48, no. 4, pp. 1154-1163, April 2000*, doi: 10.1109/78.827548.

[11] Nam-Yong Lee and B. J. Lucier, "Wavelet methods for inverting the Radon transform with noisy data," in *IEEE Transactions on Image Processing, vol. 10, no. 1, pp. 79-94, Jan. 2001*, doi: 10.1109/83.892445.

[12] J. Kalifa, A. Laine and P. D. Esser, "Regularization in tomographic reconstruction using thresholding estimators," in *IEEE Transactions on Medical Imaging, vol. 22, no. 3, pp. 351-359, March 2003*, doi: 10.1109/TMI.2003.809691.

[13] Seungseok Oh, C. A. Bouman and K. J. Webb, "Multigrid tomographic inversion with variable resolution data and image spaces," in *IEEE Transactions on Image Processing, vol. 15, no. 9, pp.2805-2819,Sept.2006*,doi: 10.1109/TIP.2006.877313.

[14] J. Guevara Escobedo and K. B. Ozanyan, "Tiled-Block Image Reconstruction by Wavelet- Based, Parallel-Filtered Back-Projection," *in IEEE Sensors Journal,* vol. 16, no. 12, pp. 4839-4846, June15, 2016, doi: 10.1109/JSEN.2016.2546182.

[15] Ge Wang and Hengyong Yu. "The meaning of interior tomography", *2013 Physics in Medicine and Biology.* 58 R161.